nature COMMUNICATIONS

ARTICLE

Received 16 Dec 2012 | Accepted 19 Jun 2013 | Published 12 Jul 2013

DOI: 10.1038/ncomms3169

Nanoporous gold supported cobalt oxide microelectrodes as high-performance electrochemical biosensors

Xing-You Lang[1,*], Hong-Ying Fu[1,*], Chao Hou[1], Gao-Feng Han[1], Ping Yang[2], Yong-Bing Liu[1] & Qing Jiang[1]

Tremendous demands for electrochemical biosensors with high sensitivity and reliability, fast response and excellent selectivity have stimulated intensive research on developing versatile materials with ultrahigh electrocatalytic activity. Here we report flexible and self-supported microelectrodes with a seamless solid/nanoporous gold/cobalt oxide hybrid structure for electrochemical nonenzymatic glucose biosensors. As a result of synergistic electrocatalytic activity of the gold skeleton and cobalt oxide nanoparticles towards glucose oxidation, amperometric glucose biosensors based on the hybrid microelectrodes exhibit multi-linear detection ranges with ultrahigh sensitivities at a low potential of 0.26 V (versus Ag/AgCl). The sensitivity up to 12.5 mA $mM^{-1} cm^{-2}$ with a short response time of less than 1 s gives rise to ultralow detection limit of 5 nM. The outstanding performance originates from a novel nanoarchitecture in which the cobalt oxide nanoparticles are incorporated into pore channels of the seamless solid/nanoporous Au microwires, providing excellent electronic/ionic conductivity and mass transport for the enhanced electrocatalysis.

[1] Key Laboratory of Automobile Materials, Ministry of Education, and School of Materials Science and Engineering, Jilin University, Changchun 130022, China. [2] Cardiovascular medicine, Sino-Japan Friendship Hospital, Jilin University, Changchun 130033, China. * These authors contributed equally to this work. Correspondence and requests for materials should be addressed to Q.J. (email: jiangq@jlu.edu.cn).

Electrochemical biosensors, which have been widely employed in clinical, environmental, industrial and agricultural applications, recognize biological analytes through a catalytic or binding event occurring at the interface of electrodes[1–5]. Intimate correlation of biosensing performance and the electrocatalytic and structural properties of electrodes has stimulated considerable efforts devoted to innovational materials to coordinate mass- and charge-transport and electron-transfer kinetics for realizing simultaneous minimization of primary resistances in biosensing: electrochemical reaction occurring at electrolyte/electrode interface, mass transport of analyte in electrolyte and electrode, and the electron conduction in electrode and current collector[6–9]. Nanostructured metal oxides have promising applications as nonenzymatic catalysts in new generation of miniaturized glucose biosensors owing to their low cost, high biocompatibility and electrocatalytic activity, as well as enhanced electron-transfer and adsorption capacities[10,11]. Judicious use of nanostructured metal oxides is expected to circumvent the key limitations of expensive enzymes, typically glucose oxidase (GOx), with compromise of the sensitivity, reproducibility and stability of glucose detection as the catalytic activity of GOx is intrinsically susceptible to environmental conditions such as temperature, humidity, pH and toxic chemicals[2,11–13]. However, the poor electronic conductivity of metal oxides (for example, Co_3O_4 in $\sim 10^{-5}\,S\,m^{-1}$ at room temperature) significantly impedes them from wide use in electrochemical biosensing devices with high sensitivity and reliability, fast response and excellent selectivity[10,14,15]. One of major strategies to enhance charge transport in electrochemical biosensors is to design composite materials by combining highly electrocatalytic materials with a conductive substance[16–20], whereas single- and multi-walled carbon nanotubes (CNTs)[21–25], graphene[26,27] and noble metal nanoparticles[28] have been explored to serve as conductive pathways of metal oxides (TiO_2, MnO_2, RuO_2, Co_3O_4 and NiO). Although these low-dimensional composite nanostructures could provide extremely large specific surface area of the electrode/electrolyte interface[16–28], the assembled electrodes exhibit an undesirably low electronic conductance as a consequence of exceptionally low electron transport in the nanomaterials as well as the high contact resistances within nanomaterials and between the current collector and electrodes[29,30], greatly hindering their potential applications in electrochemical biosensors at ultralow concentrations in unconventional body fluids.

Here we report multifunctional seamless solid/nanoporous Au/Co_3O_4 (S/NPG/Co_3O_4) hybrid microelectrodes with three-dimensional (3D) bicontinuous nanoporosity, facilely fabricated by incorporating Co_3O_4 nanoparticles onto seamless solid/nanoporous Au (S/NPG) microwires, for nonenzymatic electrochemical glucose biosensors. Amperometric measurements at a low potential demonstrate that the seamless S/NPG/Co_3O_4 microelectrodes can detect ultralow-concentration glucose with an ultrahigh sensitivity of $\sim 12.5\,mA\,mM^{-1}\,cm^{-2}$ and a fast response time of <1 s. The outstanding sensing performance results from the unique nanoarchitecture, which simultaneously minimizes the contact resistances among current collector of solid Au wire, nanoporous Au skeleton and Co_3O_4 nanoparticles. Furthermore, the nanoarchitecture provides interconnected nanoporous channels and Au ligaments, concurrently enhancing the transports of glucose and electron, and offers a large specific surface area of electrode/electrolyte interface, facilitating the full use of the enhanced electrocatalysis of Au/Co_3O_4 hybrid.

Results

Synthesis and characterization. Our fabrication strategy briefly illustrated in Fig. 1 is to combine the alloying/dealloying and hydrothermal methods, through which the preparation of seamless S/NPG microwires and the incorporation of Co_3O_4 nanoparticles into the nanopore channels are consecutively carried out. The Au microwires of 200-μm-diameter with seamless solid/nanoporous architecture (Fig. 2a) are produced by *in situ* electrochemical alloying/dealloying protocol in an electrolyte composed of $ZnCl_2$ and benzyl alcohol (BA)[31], during which Au–Zn alloys are firstly formed via the electrodeposition of zinc, and the less noble Zn is then selectively dissolved in the dealloying process for the formation of nanoporous layer with high surface area (Supplementary Fig. S1)[32]. The alloying/dealloying conditions (Supplementary Table S1) are adjusted to manipulate the resulting microstructure of nanoporous layer (Fig. 2 and Supplementary Figs S2–S5). Figure 2b,c shows representative cross-sectional and top-view scanning electron microscope images of the seamless S/NPG microwire, respectively, that is fabricated at the optimized alloying/dealloying conditions in a mixture of BA and 1.5 M $ZnCl_2$ at a scan rate of $10\,mV\,s^{-1}$ and 120 °C (the first conditions in Supplementary Table S1). The seamless solid/nanoporous structure possesses ~ 1 μm thick nanoporous layer (Fig. 2b), where a uniform and 3D bicontinuous nanoporous structure consists of quasi-periodic nanopore channels and Au ligaments with characteristic length of ~ 300 nm (Fig. 2c and Supplementary Fig. S6)[32,33]. The decreases of the cycle number, temperature, $ZnCl_2$ concentration and scan rate in the alloying/dealloying process (Supplementary Table S1) will reduce the thickness and characteristic length of nanoporous layer and change the real surface area of S/NPG skeleton, as demonstrated by scanning electron microscope micrographs and *in situ* electrochemical measurements (Supplementary Figs S2–S5,S7a and Supplementary Notes 1,2)[34].

Seamless S/NPG/Co_3O_4 hybrid microwires are synthesized by the hydrothermal method (Supplementary Table S1), wherein the loading amount and morphology of Co_3O_4 can be tailored by the $Co(NO_3)_2$ concentration (Supplementary Fig. S8) and the heating temperature (Supplementary Fig. S9), respectively. At a constant hydrothermal temperature of 180 °C, the loading amount of Co_3O_4 increases with the increasing concentration of $Co(NO_3)_2$ (Supplementary Fig. S8). In the mixed solution containing 6 mM $Co(NO_3)_2$, the well-crystallized Co_3O_4 nanoparticles uniformly and directly grow into nanopores along the Au ligaments of the seamless S/NPG microwires (Fig. 2d and Supplementary Fig. S10). The rough Co_3O_4 nanoparticles are composed of nanocrystals with diameter of ~ 5–20 nm, giving rise to a larger real surface area of S/NPG/Co_3O_4 than that of bare S/NPG (Fig. 2e and Supplementary Fig. S7). When the hydrothermal temperature increases to 260 °C, nanosheet-shaped Co_3O_4 grows vertically on Au ligaments (Supplementary Fig. S9a), whereas at

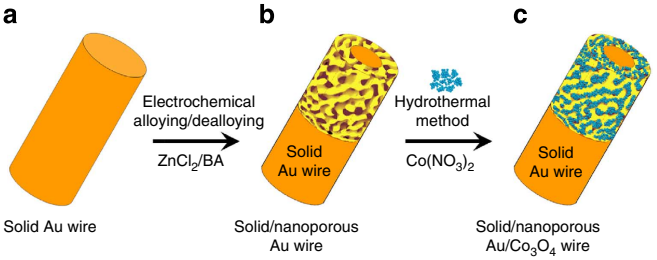

Figure 1 | Scheme for fabrication of hybrid microelectrodes. (**a**) Solid gold microwire. (**b**) 3D bicontinuous nanoporous gold layer is formed directly on the solid gold microwire by electrochemical alloying/dealloying in a mixed electrolyte of BA and $ZnCl_2$. (**c**) Co_3O_4 nanoparticles are decorated onto nanopore channels of seamless S/NPG microwire by a hydrothermal method in a mixed solution containing $Co(NO_3)_2$.

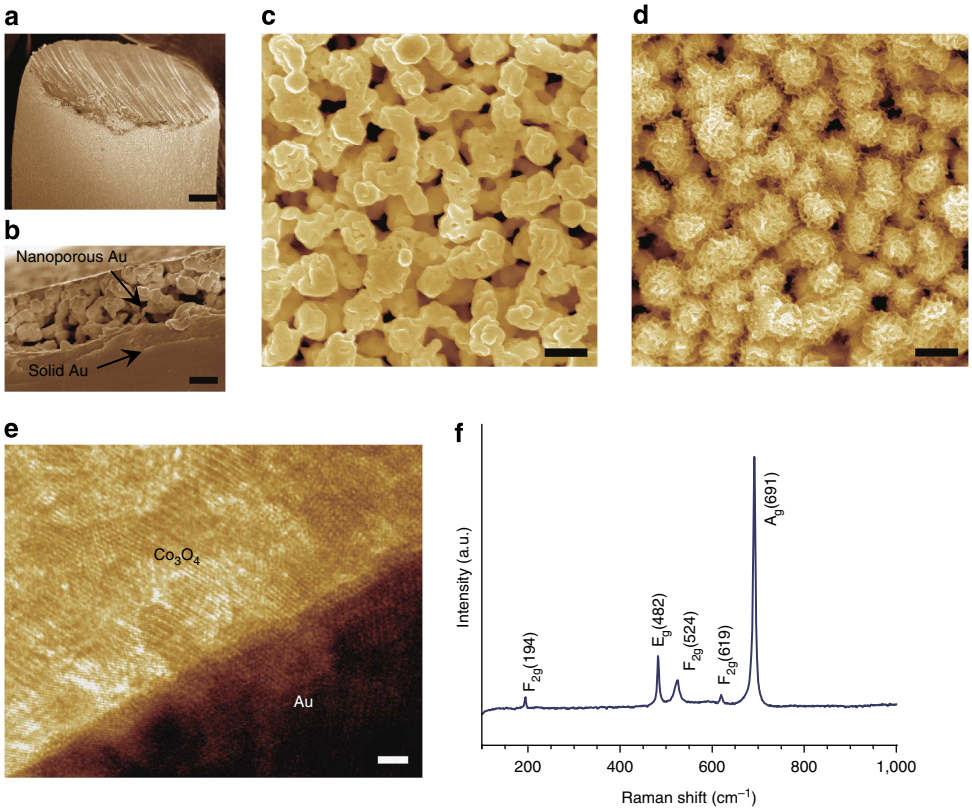

Figure 2 | Microstructure characterization. (**a**) Low-magnification and (**b**) cross-section SEM images of seamless S/NPG microwire. (**a**) Scale bar, 25 μm; (**b**) scale bar, 300 nm. Top-view SEM images of (**c**) bare S/NPG and (**d**) S/NPG/Co_3O_4 hybrid with the characteristic length of ~300 nm. (**c**,**d**) Scale bar, 300 nm. (**e**) High-resolution transmission electron microscope (HRTEM) image of Au/Co_3O_4 interfacial structure. (**e**) Scale bar, 2 nm. (**f**) Surface-enhanced Raman spectrum of seamless S/NPG/Co_3O_4 hybrid microwire.

100 °C, the formation of Co_3O_4 film seals the nanoporous structure of hybrid microelectrode (Supplementary Fig. S9c), significantly reducing the available electrolyte/electrode interface (Supplementary Fig. S7b and Supplementary Note 1). The high-resolution transmission electron microscope image of Au/Co_3O_4 interface (Fig. 2e) indicates that the Co_3O_4 nanoparticles have end-bonded contacts with the Au ligaments[29], offering excellent electrical conductivity between Au and Co_3O_4. The characteristic peaks at 194, 482, 524, 619 and 691 cm^{-1} in the surface-enhanced Raman spectrum of Co_3O_4, which are assigned to the F_{2g}, E_g, F_{2g}, F_{2g} and A_{1g} vibrational modes, respectively, unveils a spinel-type crystalline structure (Fig. 2f)[35,36]. This is further confirmed by the obvious diffraction peaks in X-ray diffraction pattern of S/NPG/Co_3O_4 hybrid corresponding to the (220), (311), (222), (400), (422), (511) and (440) planes of spinel-type Co_3O_4 (JCPDS 42–1467)[27], apart from two significant diffraction peaks at $2\theta = 44.4°$ and 77.6° attributed to the (200) and (311) reflections of Au (JCPDS 65–2870) (Supplementary Fig. S11). The direct decoration of 3D bicontinuous nanoporous Au layer on the Au microwires facilitates the integration of nanoporous metal/oxide composites with current collectors without any additional contact resistance[37]. By this technology, the entire assembled electrode not only retains excellent electrical conductivity up to the Au bulk value ($\sim 4 \times 10^5$ S cm^{-1}), much higher than those of conventional electrodes based on conducting polymers and various carbon materials, but exhibits exceptional mechanical flexibility (Supplementary Fig. S12).

Electrocatalytic activity for glucose oxidization. To assess their electrocatalytic activity, self-supported seamless S/NPG and S/NPG/Co_3O_4 microwires as well as Co_3O_4 nanoparticles (size ~5–20 nm, similar to those grown on seamless S/NPG microwire) on an ITO glass substrate (Supplementary Fig. S13a) are directly used as working electrodes for cyclic voltammetry measurements. In a N_2-bubbled mixture of 0.5 M KOH and 10 mM glucose at a scan rate of 20 mV s^{-1}, the cyclic voltammograms (CVs) for the S/NPG/Co_3O_4 microelectrodes synthesized under various alloying/dealloying and hydrothermal conditions (Supplementary Table S1) are acquired, as shown in Fig. 3 and Supplementary Figs S2d,S3–S5c,S8–S9d. Figure 3a illustrates the typical CV for S/NPG/Co_3O_4 hybrid microelectrode fabricated under the optimized alloying/dealloying and hydrothermal conditions (the first ones in Supplementary Table S1), in distinct contrast with its blank voltammetry (without glucose) (Fig. 3b) due to the glucose oxidation. In the glucose-free alkaline solution, S/NPG/Co_3O_4 concurrently presents characteristic features of both Au and Co_3O_4 nanoparticles. These include the current-density peaks of the oxidation of Au and the more negative subsequent reduction of Au oxides than that of the bare S/NPG microwire (Fig. 3b)[38]. In addition, two redox pairs of Co_3O_4 involve the reversible transition between Co_3O_4 and CoOOH via $Co_3O_4 + OH^- + H_2O \leftrightarrow 3CoOOH + e^-$ and the further conversion between CoOOH and CoO_2 via $CoOOH + OH^- \leftrightarrow CoO_2 + H_2O + e^-$ (Supplementary Fig. S13b)[15,27]. For comparison, the CVs of the corresponding S/NPG microwire and Co_3O_4 nanoparticles in 0.5 M KOH with and without 10 mM glucose are also included in Fig. 3a,b, and Supplementary Fig. S13b, respectively, presenting low electrocatalytic activities[15,27,38,39]. Remarkably, the CV of the seamless S/NPG/Co_3O_4 hybrid microelectrode shows a much more negative onset potential and higher anodic current density

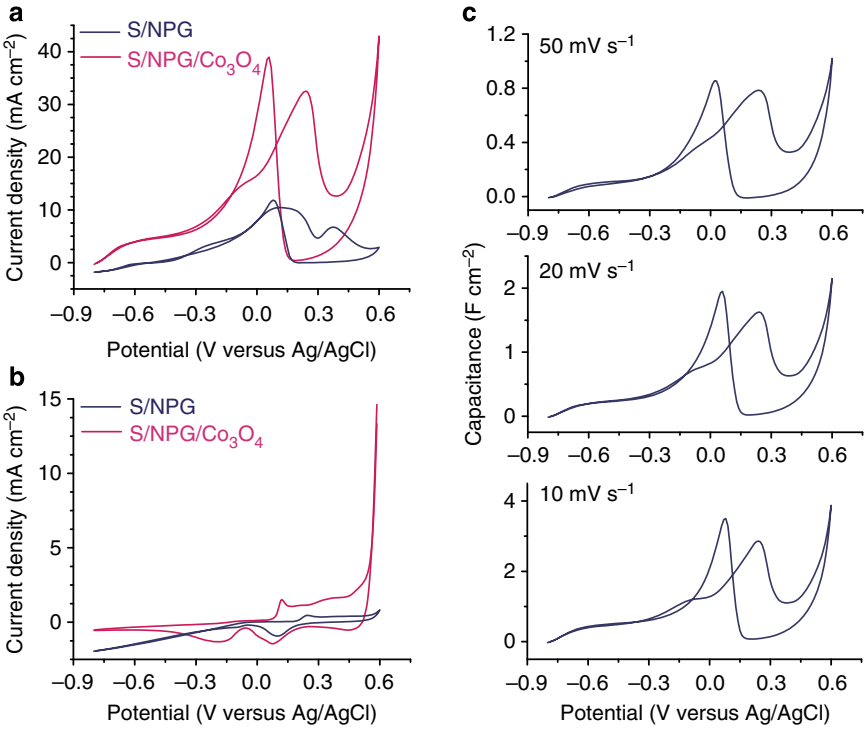

Figure 3 | Electrochemical characterization. Cyclic voltammetry (CV) curves of seamless S/NPG and S/NPG/Co_3O_4 hybrid microelectrodes in 0.5 M KOH (**a**) with and (**b**) without 10 mM glucose at a scan rate of 20 mV s^{-1}. (**c**) CV profiles of the seamless S/NPG/Co_3O_4 wire electrode at different scan rates. Current axis in **c** is scaled by the scan rate.

than those of the bare seamless S/NPG microwire and the Co_3O_4 nanoparticles (Fig. 3a and Supplementary Fig. S13b), suggesting synergistic electrocatalytic activity of S/NPG and Co_3O_4 in the hybrid towards glucose electrooxidation. As shown in Fig. 3a, the voltammetric behaviour of the seamless S/NPG/Co_3O_4 hybrid microelectrode in the low potential range ($< \sim -0.06$ V) produces a substantially enhanced current response as a result of glucose electrosorption[28,38,40]. This takes place on the significantly increased electroactive surface sites to form the adsorbed intermediates by releasing one proton per glucose molecule at an onset potential of ~ -0.78 V (much more negative than ~ -0.49 V for bare S/NPG microwire). Accompanying by electrosorption of glucose, the accumulation of the concomitant intermediates on the electrode surface inhabits direct oxidation of glucose on the active sites of Au hence gives rise to the small anodic current peak at ~ -0.06 V (refs 28,38,40). Meanwhile, Co_3O_4 nanoparticles hybridized with seamless S/NPG microwire intervene in a catalytical promotion of glucose oxidation (Supplementary Fig. S13b), leading to the continuous increase of the current. At higher positive potentials, both AuOH and CoOOH form on the internal surface of seamless S/NPG/Co_3O_4 electrode by the partial discharge of OH^-, and consequently catalyse the oxidation of intermediates and the direct oxidation of glucose[27,28,38,40] by the conversions of $AuOH \rightarrow Au$ and $CoOOH \rightarrow Co_3O_4$, respectively. The corresponding broad anodic current peak is at $\sim$0.25 V. When the potential sweeps more positively, the current density decreases in the potential range of 0.25–0.39 V as formation of Au oxides suppresses the direct electrooxidation of glucose[28,38,40]. Upon the potential higher than $\sim$0.39 V, the current density dramatically increases as a result of the formation of CoO_2 on which direct glucose oxidation occurs via $CoO_2 + C_6H_{12}O_6 \rightarrow CoOOH + C_6H_{10}O_6$ (refs 15,27). In the negative scan, Au oxides are reduced and a large number of active sites on the internal surface of seamless S/NPG/Co_3O_4 electrode are regenerated for the direct glucose oxidation, leading to an anodic current peak at $\sim$0.05 V (refs 28,38). When Co_3O_4 nanoparticles are incorporated into the S/NPG skeleton with a larger characteristic-length and thinner NPG layer (Supplementary Note 2) at the same hydrothermal conditions (Supplementary Figs S2–S5 and Supplementary Table S1), the CV of S/NPG/Co_3O_4 hybrid microelectrode shows a lower anodic current density and a less negative onset potential (Supplementary Figs S2d,S3c–S5c) because of less surface area for the formation of highly active Au/Co_3O_4 hybrid (Supplementary Fig. S7a). This demonstrates the important role of high nanoporosity of S/NPG skeleton in producing a large amount of Au/Co_3O_4 hybrid which significantly enhances the electrocatalytic activity of the whole hybrid microelectrodes.

Furthermore, the enhanced electrocatalytic behaviour of seamless S/NPG/Co_3O_4 hybrid microelectrodes is found to rely significantly on the scan rate (Fig. 3c). For lower scan rates, comparatively more glucose is electrooxidized at the surface, indicating a surface-controlled electrochemical process. This is further verified by the observation that the smaller the surface area of S/NPG/Co_3O_4 microelectrodes, the lower the current densities (Supplementary Figs S7b,S9d). It is noteworthy that the change of the surface area results from the evolution of morphology and loading amount of Co_3O_4 on the same S/NPG microwires at different hydrothermal conditions (Supplementary Table S1). The current density of S/NPG/Co_3O_4 hydrothermally synthesized at 100 °C falls dramatically as the nanoporous structure is sealed by the Co_3O_4 film (Supplementary Fig. S9c,d), which restrains ion and glucose transports as well as the availability of electrolyte/electrode interface for glucose electrooxidation.

Amperometric glucose detection. For all S/NPG and S/NPG/Co_3O_4 microelectrodes (Supplementary Table S1), the glucose

sensing performance is evaluated by amperometric measurements, and their current-time curves for successive addition of glucose with concentrations ranging from 1 μM to 10 mM are recorded at an applied potential of 0.26 V (Fig. 4 and Supplementary Fig. S14). As a result of the enhanced electrocatalytic activities of hybrid nanoarchitecture towards glucose oxidation, the current responses and sensitivities of S/NPG/Co_3O_4 microelectrodes are enhanced by increasing the surface areas of both the S/NPG skeletons and their Co_3O_4 hybrids (Supplementary Figs S14,S15). The former affords more Au/Co_3O_4 interface for enhancing the electrochemical activity of Co_3O_4 and improving the electron transport of Co_3O_4 to Au network, whereas the latter enables to trap more molecules for electrooxidation and to provide the large surface area of electrolyte/electrode interface for the full use of highly active Au/Co_3O_4 hybrid.

Figure 4 gives the typical comparisons of amperometric responses between bare S/NPG and S/NPG/Co_3O_4 hybrid microelectrodes synthesized at the optimized alloying/dealloying and hydrothermal conditions (the first ones in Supplementary Table S1). Owing to the synergistic electrocatalytic activity of Au/Co_3O_4 hybrid nanostructure and the excellent conductivity of seamless solid/nanoporous architecture, the amperometric response of the seamless S/NPG/Co_3O_4 hybrid microelectrode exhibits perfect and stable step curve with dramatically enhanced current density in comparison with that of bare S/NPG (Fig. 4a). It should be noted that a response time no more than 1 s to research 95% of steady-state current (Fig. 4c and Supplementary Fig. S16a) is much faster than 2 s for nanometal-decorated graphite nanoplatelet[19], 6 s for GOx-CNT networks[41] or 7 s for porous Co_3O_4 nanofibers[15]. In consequence, incorporating Co_3O_4 nanoparticles into the 3D bicontinuous nanoporous gold of seamless solid/nanoporous structure remarkably improves the glucose sensing ability compared with the bare seamless S/NPG microwire as well as free Co_3O_4 nanoparticles (Fig. 4a and Supplementary Fig. S13c), which is further verified by their calibration curves (Fig. 4b and Supplementary Fig. S13d). As illustrated in the current density versus concentration plots (Supplementary Figs S16–S18), the glucose biosensors based on Co_3O_4 nanoparticles, seamless S/NPG and S/NPG/Co_3O_4 hybrid microelectrodes show multi-linear detection ranges with different sensitivities up to 7, 30 and 70 mM, respectively, displaying a strong dependence on the concentration of added glucose (Fig. 4d). As the concentration decreases to 1 μM, the sensitivity of seamless S/NPG/Co_3O_4 hybrid increases up to $\sim 12.5\ mA\ mM^{-1}\ cm^{-2}$, much higher than the values of bare seamless S/NPG ($0.72\ mA\ mM^{-1}\ cm^{-2}$) (Fig. 4d) and Co_3O_4 nanoparticles (Supplementary Fig. S13). Such an ultrahigh sensitivity offers the seamless S/NPG/Co_3O_4 microelectrode a remarkably low detection limit of 5 nM (Fig. 5a), much lower than some of the lowest values reported previously: 970 nM for electrospun Co_3O_4 nanofibers[15], 25 nM for 3D graphene/Co_3O_4 composite[27] or 1.29 μM for the GOx-immobilized one-dimensional TiO_2 nanostructure[21]. Moreover, the seamless S/NPG/Co_3O_4 microelectrode provides superb selectivity for glucose detection at the low applied potential of 0.26 V, which minimizes the responses of common interference species such as uric acid, acetamidophenol and ascorbic acid, in physiological levels[38,42], as well as other sugars including fructose, mannose, maltose, sucrose and lactose[42]. Addition of 0.02 mM uric acid, 0.1 mM acetamidophenol, ascorbic acid or other sugars to a 1-mM glucose solution results in only ~0.5–5% increase in the current density, and does not interfere with the glucose detection even without the permselective coatings (Fig. 5b and

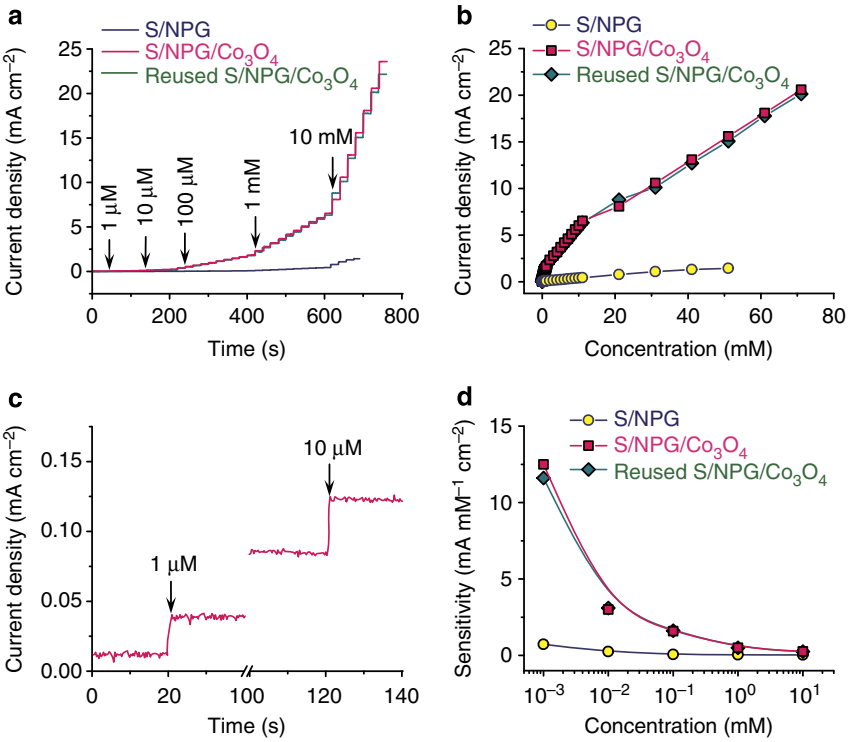

Figure 4 | Amperometric glucose detection. (**a**) Chronoamperometry curves and (**b**) the calibration curves (current density versus glucose concentration) for the amperometric responses of seamless S/NPG and fresh and reused S/NPG/Co_3O_4 microelectrodes to the successive addition of glucose with the concentrations from 1 μM to 10 mM in 0.5 M KOH solution at a constant potential of 0.26 V (versus Ag/AgCl). (**c**) Fast response of seamless S/NPG/Co_3O_4 hybrid microelectrode to 1 and 10 μM glucose. (**d**) Glucose sensitivities of seamless S/NPG and fresh and reused S/NPG/Co_3O_4 microelectrodes as a function of the concentration of glucose.

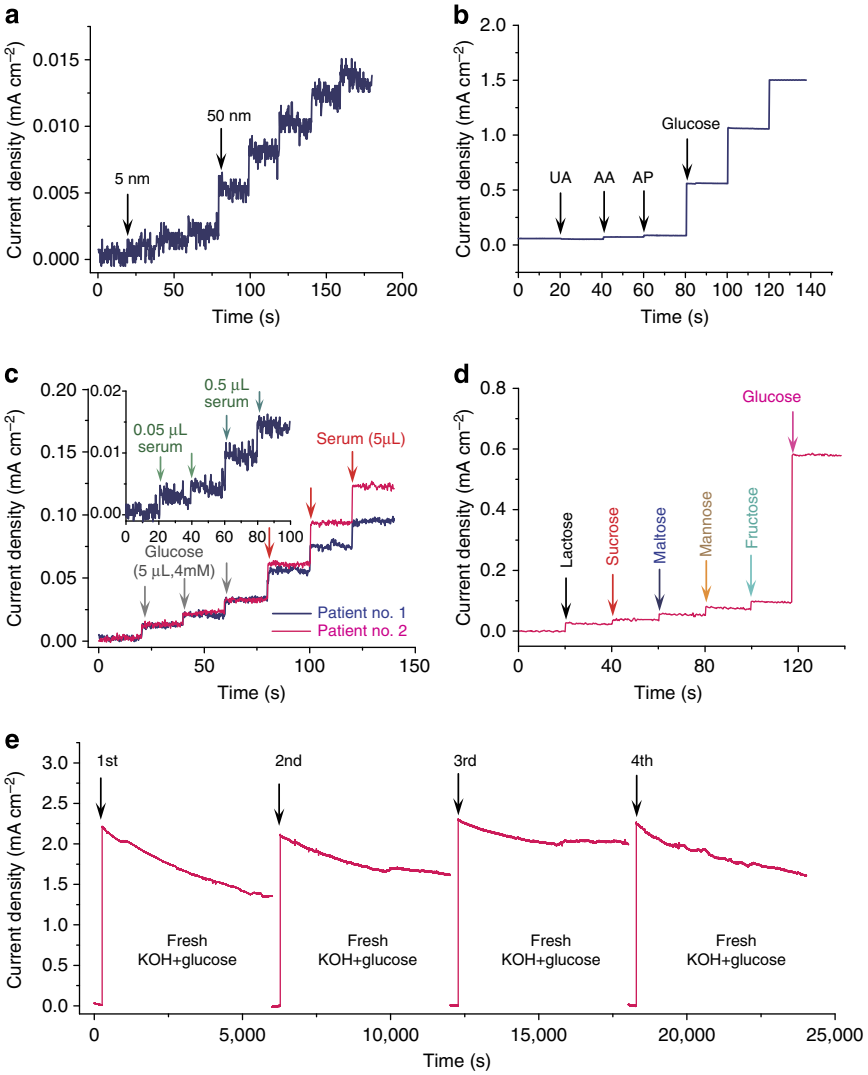

Figure 5 | Selectivity and stability. (**a**) Amperometric response to glucose with the low limit concentrations of 5 and 50 nM. Amperometric response to the successive addition of interfering compounds such as (**b**) 0.02 mM uric acid (UA), 0.1 mM acetamidophenol (AP), 0.1 mM ascorbic acid (AA) and (**d**) 0.1 mM fructose, mannose, maltose, sucrose, lactose, as well as 1 mM glucose at a potential of 0.26 V. (**c**) Current response of the S/NPG/Co_3O_4 microelectrode to successive three-time additions of 5 µl glucose (4 mM) and blood serum of two diabetic patients into 20 ml 0.5 M electrolyte. Inset: Current response of the S/NPG/Co_3O_4 microelectrode stored at room temperature for 4 months to ultralow concentration of serum. (**e**) Current-time curve for the S/NPG/Co_3O_4 at 0.26 V in four fresh electrolytes containing 0.5 M KOH and 10 mM glucose.

Supplementary Table S2). These predominant properties enlist this hybrid microelectrode to exhibit high reliability for analysing blood serums. Figure 5c demonstrates the current-time curves for the successive additions of 5 µl 4 mM glucose standard solution and 5 µl blood serums of diabetic patients into 20 ml 0.5 M KOH solution, according to which the measured blood-glucose concentrations of diabetic patients are consistent with the values reported by the clinical analysis in the hospital (Supplementary Table S3).

The electrochemical stability of the S/NPG/Co_3O_4 hybrid microelectrode is investigated by the chronoamperometric method in four fresh solutions containing 0.5 M KOH and 10 mM glucose (Fig. 5d). In spite of the slow decrease of the current with time, the starting current response maintains stable in each fresh electrolyte, revealing the good stability of the hybrid microelectrodes during the electrochemical measurements. This is also confirmed by UV–visible spectrum of the measurement solution, where no Co or Au ion is detected (Supplementary Fig. S19). Moreover, the aging tolerance ensures the S/NPG/Co_3O_4 hybrid microelectrode to retain ~99.5% of its original current response over a storage period of 15 days at room temperature (Supplementary Fig. S20), indicating the excellent reproducibility with a relative s.d. of ~0.6%. Even the S/NPG/Co_3O_4 hybrid microelectrode stored at room temperature for 4 months still maintains the high capability to analyse serum sample at ultralow concentrations (inset of Fig. 5c).

To demonstrate the reusability, an S/NPG/Co_3O_4 hybrid microelectrode is reconstructed via a procedure: etching the used S/NPG/Co_3O_4 microelectrode in concentrated HNO_3 to remove Co_3O_4 (Supplementary Fig. S21a), and then reincorporating Co_3O_4 nanoparticles onto the used S/NPG microwire by hydrothermal method (Supplementary Fig. S21b). The amperometric response of the reused S/NPG/Co_3O_4 microelectrode to the successive addition of glucose shows outstanding glucose sensing performance comparable to the as-prepared one (Fig. 4a,b,d, and Supplementary Fig. S22), indicating its superior

reusability and reproducibility. Thus, the seamless S/NPG/Co_3O_4 hybrid microelectrode is an excellent material for the enhanced electrochemical sensing.

Discussion

In the perspective of the Langmuir isothermal theory for surface electrocatalytic reaction[15], the sensitivity (m) of seamless S/NPG/Co_3O_4 microelectrode is governed by the glucose concentration (C_g) (as shown in Fig. 4d), namely, $m = di_T/dC_g = K_B K_A C_a/(1 + K_A C_g)^2$, where the total current density $i_T = K_B C_{gS}$ with $C_{gS} = K_A C_g C_a/(1 + K_A C_g)$ being the concentration of glucose adsorbed on the catalyst surface, C_a denotes the molar concentration of active sites on the catalyst, K_A and K_B are the adsorption equilibrium constant and the reaction rate constant, respectively[15]. As C_g is low enough (1 μM), that is, $1 \ll K_A C_g$, $m_L \approx K_B K_A C_a = 12.5\,mA\,mM^{-1}\,cm^{-2}$, indicating the intrinsically ultrahigh electrocatalytic activity of seamless S/NPG/Co_3O_4 hybrid microelectrode towards glucose oxidation due to the unique nanoarchitecture of seamless S/NPG skeleton and synergistic Au/Co_3O_4 hybrid. The seamless S/NPG framework, ingeniously integrating NPG layer with current collector by directly alloying/dealloying process on Au wire, minimizes the contact resistance between NPG layer and current collector, and thus optimizes the sensing performance in comparison with NPG species binded to current collector by polymer binders or adhesives (Supplementary Fig. S23)[38]. Meanwhile, the 3D open and bicontinuous nanoporous structure provides a large room for loading Co_3O_4 nanoparticles, and the produced nanoporous Au/Co_3O_4 hybrid with extremely large specific surface area enhances the mass transport kinetics and facilitates sufficient use of the highly active Au/Co_3O_4 hybrid[6,7,9]. Therefore, the thicker the NPG layer with the same characteristic length (Supplementary Note 2), the higher the glucose sensitivity of S/NPG/Co_3O_4 hybrid microelectrode (Supplementary Fig. S24). Although free nanostructured Co_3O_4 has intrinsically ultralow conductivity that limits its application in biosensing (Supplementary Figs S13,S18)[15], the nanoporous Au/Co_3O_4 hybrid substantially enhances the electron transfer and improves the electrocatalytic activity of Co_3O_4 (m_{Co3O4}), which is approximately calculated by subtracting the value of NPG (m_{NPG}) according to the equation $m_{Co3O4} = m_L - m_{NPG} = 11.72\,mA\,mM^{-1}\,cm^{-2}$, two orders of magnitude higher than that of porous Co_3O_4 nanofibers[15]. This great enhancement allows the seamless S/NPG/Co_3O_4 microelectrode to detect glucose at ultralow concentrations with exquisite selectivity for potential applications in monitoring glucose in conventional and unconventional body fluids, as well as complementing or even replacing the GOx-based biosensors outside their rigorous operational environments (high temperature, high pH and so on). Additionally, the facile collection and reusability of S/NPG and S/NPG/Co_3O_4 microwires can dramatically reduce the cost of Au/Co_3O_4-based biosensing devices, meeting low-cost requirements for the large-scale biosensing use.

In summary, by the facile two-step procedure involving electrochemical alloying/dealloying and hydrothermal synthesis we have developed a seamless microelectrode with hybrid nanoarchitecture of S/NPG/Co_3O_4 as a promising electrode material for high-performance electrochemical biosensors with ultrahigh sensitivity and ultrafast response time. The impressive glucose sensing behaviour of seamless S/NPG/Co_3O_4 hybrid microelectrodes originates from the substantially enhanced electrocatalytic activity of the Au/Co_3O_4 hybrid and the unique seamless solid/porous nanoarchitecture, which simultaneously minimizes the primary resistances in biosensing, viz. the electrochemical reaction occurring at electrode/electrolyte interfaces, the mass transport of analyte in electrolyte and electrode, and the electron conduction in electrode and current collector.

Methods

Fabrication of seamless microwires. The seamless S/NPG wires were prepared by a multicyclic electrochemical alloying/dealloying method based on a three-electrode electrochemical cell (Iviumstat electrochemical analyzer, Ivium Technology), in which Zn plate and wire were used as the auxiliary electrode and the reference electrode in a BA electrolyte containing 1.5 M $ZnCl_2$, respectively[31]. 3D bicontinuous nanoporous layer with tunable microstructural features was decorated on polished Au wires with diameters of ~200 μm after the electrochemical cycles in the potential range from −0.72 to 1.88 V (versus Zn) at different conditions (Supplementary Table S1)[31]. After acetone, ethanol and deionized water (18.2 MΩ cm) rinsing in sequence, the seamless S/NPG wire fixed on a plastic clamp was moved into the Teflon-lined stainless steel autoclave filled with the mixture of 3, 6, 9 mM $Co(NO_3)_2$, 2 mM cetyltrimethylammonium bromide, 5 ml pure water and 30 ml ethanol. The sealed autoclave was heated in an electric oven at 100, 180 and 260 °C for 90 min for synthesis of the seamless Au/NPG/Co_3O_4 (Supplementary Table 1S). After cooled to room temperature, the hybrid wire was washed with deionized water. The S/NPG microwire was collected from the tested S/NPG/Co_3O_4 microelectrode via chemical etching in 60% HNO_3 for the further reconstruction of S/NPG/Co_3O_4 microelectrode via hydrothermal method at the first conditions in Supplementary Table S1.

Characterization. The microstructure and chemical composition of the specimens were investigated using a field-emission transmission electron microscope (JEOL JEM-2100F, 200 keV), and a field-emission scanning electron microscope (JEOL, JSM-6700F, 15 keV) equipped with an X-ray energy-dispersive microscopy. Raman spectrum was collected using a micro-Raman spectrometer (Renishaw) with a laser of 532 nm wavelength. X-ray diffraction measurement was carried out on a D/max2500pc diffractometer using Cu $K\alpha$ radiation.

Electrochemical Measurement. All cyclic voltammetry and amperometric experiments were performed in a three-electrode setup, which employed gold wire, seamless Au/NPG, Au/NPG/Co_3O_4 microwires and Co_3O_4 nanoparticles supported on ITO glass as the working electrodes, a Pt foil electrode as the counter electrode and a Ag/AgCl electrode as the reference electrode, in the 0.5 M KOH electrolyte bubbled by nitrogen gas for 30 min. The CVs were collected in the aqueous electrolyte with and without 10 mM glucose. The amperometric responses of microelectrodes to serum and glucose with different concentrations ranging from 1 μM to 10 mM were recorded under steady-state conditions at a potential of 0.26 V (versus Ag/AgCl). The concentration of blood glucose of diabetic patients was measured by automatic biochemical analyzer (Bakeman Coulter DXC800).

References

1. Ronkainen, N. J., Halsall, H. B. & Heineman, W. R. Electrochemical biosensors. *Chem. Soc. Rev.* **39,** 1747–1763 (2010).
2. Wang, J. Electrochemical glucose biosensors. *Chem. Rev.* **108,** 814–825 (2008).
3. Chen, R. J. *et al.* An investigation of the mechanisms of electronic sensing of protein adsorption on carbon nanotube devices. *J. Am. Chem. Soc.* **126,** 1563–1568 (2004).
4. Im, H., Huang, X. J., Gu, B. & Choi, Y. K. A dielectric-modulated field-effect transistor for biosensing. *Nat. Nanotech.* **2,** 430–434 (2007).
5. Xiang, Y. & Lu, Y. Using personal glucose meters and functional DNA sensors to quantify a variety of analytical targets. *Nat. Chem.* **3,** 697–703 (2011).
6. Kissinger, P. T. & Heineman, W. R. *Laboratory Techniques in Electroanalytical Chemistry* (Marcel Dekker Inc, New York, 1996).
7. Yang, W. *et al.* Carbon nanomaterials in biosensors: should you use nanotubes or graphene? *Angew. Chem. Int. Ed.* **49,** 2114–2138 (2010).
8. Šljukić, B., Banks, C. E. & Compton, R. G. Iron oxide particles are the active sites for hydrogen peroxide sensing at multiwalled carbon nanotube modified electrodes. *Nano. Lett.* **6,** 1556–1558 (2006).
9. Minteer, S. D., Atanassov, P., Luckarift, H. R. & Johnson, G. R. New materials for biological fuel cells. *Mater. Today* **15,** 166–173 (2012).
10. Solanki, P. R., Kaushik, A., Agrawal, V. V. & Malhotra, B. D. Nanostructured metal oxide-based biosensors. *NPG Asia Mater.* **3,** 17–24 (2011).
11. Kimmel, D. W., LeBlanc, G., Meschievitz, M. E. & Cliffel, D. E. Electrochemical sensors and biosensors. *Anal. Chem.* **84,** 685–707 (2012).
12. Wilson, R. & Turner, A. P. F. Glucose oxidase: an ideal enzyme. *Biosens. Bioelectron.* **7,** 165–185 (1992).
13. Wang, J. P., Thomas, D. F. & Chen, A. C. Nonenzymatic electrochemical glucose sensor based on nanoporous PtPb networks. *Anal. Chem.* **80,** 997–1004 (2008).
14. Duan, H. M., Xu, D. Y., Li, W. Z. & Xu, H. Y. Study of the redox properties of noble metal/Co_3O_4 by electrical conductivity measurements. *Catal. Lett.* **124,** 318–323 (2008).

15. Ding, Y. *et al.* Electrospun Co_3O_4 nanofibers for sensitive and selective glucose detection. *Biosens. Bioelectron.* **26,** 542–548 (2008).
16. Kros, A., Nolte, R. J. M. & Sommerdijk, N. A. J. M. Conducting polymers with confined dimensions: track-etch membranes for amperometric biosensor applications. *Adv. Mater.* **14,** 1779–1782 (2002).
17. Besteman, K., Lee, J., Wiertz, F. G. M., Heering, H. A. & Dekker, C. Enzyme-coated carbon nanotubes as single-molecule biosensors. *Nano Lett.* **3,** 727–730 (2003).
18. Willner, I. & Willner, B. Biomolecule-based nanomaterials and nanostructures. *Nano Lett.* **10,** 3805–3815 (2010).
19. Lu, J., Do, I., Drzal, L. T., Worden, R. M. & Lee, I. Nanometal-decorated exfoliated graphite nanoplatelet based glucose biosensors with high sensitivity and fast response. *ACS Nano* **2,** 1825–1832 (2008).
20. Guo, S. J., Wen, D., Zhai, Y. M., Dong, S. J. & Wang, E. K. Platinum nanoparticle ensemble-on-graphene hybrid nanosheet: one-pot, rapid synthesis, and used as new electrode materials for electrochemical sensing. *ACS Nano* **4,** 3959–3968 (2010).
21. Si, P., Ding, S. J., Yuan, J., Lou, X. W. & Kim, D. H. Hierarchically structured one-dimensional TiO_2 for protein immobilization, direct electrochemistry, and mediator-free glucose sensing. *ACS Nano* **5,** 7617–7626 (2011).
22. Chen, J., Zhang, W. D. & Ye, J. S. Nonenzymatic electrochemical glucose sensor based on MnO_2/MWNTs nanocomposite. *Electrochem. Commun.* **10,** 1268–1271 (2008).
23. Tehrani, R. M. A. & Ghani, S. A. MWCNT-ruthenium oxide composite paste electrode as non-enzymatic glucose sensor. *Biosens. Bioelectron.* **38,** 278–283 (2012).
24. Campuzano, S. & Wang, J. Nanobioelectroanalysis based on carbon/inorganic hybrid nanoarchitectures. *Electroanalysis* **23,** 1289–1300 (2011).
25. Reddy, A. L. M., Shaijumon, M. M., Gowda, S. R. & Ajayan, P. M. Coaxial MnO_2/carbon nanotube array electrodes for high-performance lithium batteries. *Nano Lett.* **9,** 1002–1006 (2009).
26. Ye, D. X., Luo, L. Q., Ding, Y. P., Liu, B. D. & Liu, X. Fabrication of Co_3O_4 nanoparticles-decorated graphene composite for determination of L-tryptophan. *Analyst* **137,** 2840–2845 (2012).
27. Dong, X. C. *et al.* 3D graphene-cobalt oxide electrode for high-performance supercapacitor and enzymeless glucose detection. *ACS Nano* **6,** 3206–3213 (2012).
28. Ding, Y., Liu, Y. X., Parisi, J., Zhang, L. C. & Lei, Y. A novel NiO-Au hybrid nanobelts based sensor for sensitivie and selective glucose detection. *Biosens. Bioelectron.* **28,** 393–398 (2011).
29. Léonard, F. & Talin, A. A. Electrical contacts to one- and two-dimensional nanomaterials. *Nat. Nanotech.* **6,** 773–783 (2011).
30. Gowda, S. R., Reddy, A. L. M., Zhan, X. B., Jafry, H. R. & Ajayan, P. M. 3D nanoporous nanowire current collectors for thin films microbatteries. *Nano Lett.* **12,** 1198–1202 (2012).
31. Yu, C. F., Jia, F. L., Ai, Z. H. & Zhang, L. Z. Direct oxidation of methanol on self-supported nanoporous gold film electrodes with high catalytic activity and stability. *Chem. Mater.* **19,** 6065–6067 (2007).
32. Erlebacher, J., Aziz, M. J., Karma, A., Dimitrov, N. & Sieradzki, K. Evolution of nanoporosity in dealloying. *Nature* **410,** 450–453 (2001).
33. Fujita, T. *et al.* Unusually small electrical resistance of three-dimensional nanoporous gold in external magnetic fields. *Phys. Rev. Lett.* **101,** 166601 (2008).
34. Trasatti, S. & Petrii, O. A. Real surface area measurements in electrochemistry. *Pure Appl. Chem.* **63,** 711–734 (1991).
35. Yeo, B. S. & Bell, A. T. Enhanced activity of gold-supported cobalt oxide for the electrochemical evolution of oxygen. *J. Am. Chem. Soc.* **133,** 5587–5593 (2011).
36. Yang, J., Liu, H. W., Martens, W. N. & Frost, R. L. Synthesis and characterization of cobalt hydroxide, cobalt oxyhydroxide, and cobalt oxide nanodics. *J. Phys. Chem. C* **114,** 111–119 (2010).
37. Lang, X. Y., Hirata, A., Fujita, T. & Chen, M. W. Nanoporous metal/oxide hybrid electrodes for electrochemical supercapacitors. *Nat. Nanotech.* **6,** 232–236 (2011).
38. Chen, L. Y., Fujita, T., Ding, Y. & Chen, M. W. A three-dimensional gold-decorated nanoporous copper core-shell composite for electrocatalysis and nonenzymatic biosensing. *Adv. Funct. Mater.* **20,** 2279–2285 (2010).
39. Fujita, T. *et al.* Atomic origins of the high catalytic activity of nanoporous gold. *Nat. Mater.* **11,** 775–780 (2012).
40. Aoun, S. B. *et al.* Effect of metal ad-layers on Au(111) electrodes on electrocatalytic oxidation of glucose in an alkaline solution. *J. Electroanal. Chem.* **567,** 175–183 (2004).
41. Claussen, J. C., Franklin, A. D., Haque, A. U., Porterfield, D. M. & Fisher, T. S. Electrochemical biosensor of nanocube-augmented carbon nanotube networks. *ACS Nano* **3,** 37–44 (2009).
42. Toghill, E. E. & Compton, R. G. Electrochemical non-enzymatic glucose sensors: a perspective and evaluation. *Int. J. Electrochem. Soc.* **5,** 1246–1301 (2010).

Acknowledgements

This work was supported by the National Natural Science Foundation of China (no. 51201069, 81270315), the National Key Basic Research Development Program (no. 2010CB631001), the Keygrant Project of Chinese Ministry of Education (no. 313026), the Program for New Century Excellent Talents in University (no. NCET-10-0437) and the Research Fund for the Doctoral Program of Higher Education of China (no. 20120061120042).

Author contributions

X.-Y.L., H.-Y.F. and Q.J. conceived and designed the experiments. X.-Y.L., H.-Y.F., C.H., G.-F.H. carried out the fabrication of materials and performed electrochemical and microstructural characterizations. X.-Y.L., H.-Y.F. and Q.J. wrote the paper, and all authors discussed the results and commented on the manuscript.

Additional information

Supplementary Information accompanies this paper at http://www.nature.com/naturecommunications

Competing financial interests: The authors declare no competing financial interests.

Reprints and permission information is available online at http://npg.nature.com/reprintsandpermissions/

How to cite this article: Lang, X.-Y. *et al.* Nanoporous gold supported cobalt oxide microelectrodes as high-performance electrochemical biosensors. *Nat. Commun.* 4:2169 doi: 10.1038/ncomms3169 (2013).